Acta Astronautica 215 (2024) 455–463

Contents lists available at ScienceDirect

Acta Astronautica

journal homepage: www.elsevier.com/locate/actaastro

Numerical analysis of *n*-octadecane melting process in a rectangular cell under reboosting maneuver conditions

D. Dubert [a,*], M.J. Simón [b], J. Massons [a], X. Ruiz [a], Jna Gavaldà [a]

[a] Departament de Química Física i Inorgànica, Universitat Rovira i Virgili, Tarragona, Spain
[b] Departament d'Enginyeria Mecànica, Universitat Rovira i Virgili, Tarragona, Spain

ARTICLE INFO

Keywords:
Phase change materials
Thermocapillary convection (marangoni effect)
ISS vibrational environment
OpenFoam software

ABSTRACT

The improvement of heat management based on Phase Change Materials (PCMs) is of increasing importance in space environments. In this context, a future ESA project called "Effect of Marangoni Convection on heat transfer in Phase Change Materials (MarPCM)" will evaluate the degree of improvement in heat transport using thermocapillarity as convective activator of the liquid phase generated during the melting. Since this type of project needs to be performed onboard International Space Station, ISS, it is of outmost importance to know if the accelerometric environment of the Station could affect the experiment results.

To do so, various 2D simulations of the solid-liquid phase change were carried out using *n*-octadecane as PCM material, by considering a pre-selected acceleration signal coming from a real ISS reboosting maneuver (June 24, 2021). Different gravity scenarios have been considered by changing both the intensity and the orientation of the reboosting maneuver, parallel (x direction) and perpendicular (y direction) to the thermal gradients. The acceleration levels were enhanced up to 1000 times the intensity achieved during the real reboosting in order to predict the safety margins of the ISS experiment.

The results showed alterations of the liquid-solid interface, during the melting process in the high g-level scenarios considered. In these cases, the oscillatory flow pattern became more complex detecting sudden changes in the main frequency which were maintained approximately 1000 s after the reboosting ended. Nevertheless, applying real boosting maneuver no significant influence in the melting process was detected.

1. Introduction

The importance of efficient energy management has risen in the last years due to the limited reserves of fossil fuels and the continuous concern on the greenhouse gas increment. An effective usage of energy became, thus, a key objective for many domestic and industrial sectors [1–3]. Specifically, in thermal energy storage aspects, there are two possible alternatives involving the use of sensible or latent heat of a given material. These alternatives can be achieved by cooling, heating, melting, solidifying, condensing or vaporizing the material. It has been demonstrated that the latent heat storage is most efficient as undergoes solid-gas, solid-liquid or liquid-gas phase change or viceversa. Usually, when PCM melts it absorbs the energy and when solidifies it releases this energy [2]. In case of solid/liquid transitions, a considerable range of Phase Change Materials (PCMs) have been analyzed due to their technological advantages. Among these, polymer-based PCMs, such as paraffins, achieved large interest due to their properties. The devices built out of these PCMs are cheap, sustainable and enable extraordinarily simple and robust designs [4,5].

In space, thermal fluctuations are more important than on Earth, as spacecrafts must deal with significant changes in temperature, therefore, designing a simple and efficient thermal control system is necessary. Within this perspective, solid/liquid PCM materials became widely recognized as an important tool for optimizing thermal control [6,7]. PCM's space applications have been already used in Lunar Roving Vehicle systems from NASA's Apollo missions [8], by keeping the electronic devices in their safe temperature range (thermal control of satellites) or in heat exchangers onboard space stations and spacecrafts [7,9–11]. Extending the investigation line for optimizing the PCMs performance in low gravity (parabolic flights) environments [12,13], the European Space Agency (ESA) recently approved the project called "Effect of Marangoni Convection on heat transfer in Phase Change Materials, MarPCM" to be carried out onboard International Space Station (ISS) during the next following years. Its main objective focuses on the

* Corresponding author.
E-mail address: dianacristina.dubert@urv.cat (D. Dubert).

https://doi.org/10.1016/j.actaastro.2023.12.020
Received 18 October 2023; Received in revised form 5 December 2023; Accepted 10 December 2023
Available online 15 December 2023

Table 1
Thermophysical properties of the *n*-octadecane [23,24].

Property	Symbol	Value
Density [kg/m3]	ρ	780
Dynamic viscosity [kg/m.s]	μ	0.0035
Thermal conductivity [W/m.K]	λ_L/λ_S	0.13/0.358
Specific heat [J/kg.K]	C_L/C_S	2196/1934
Melting/solidification temperature [K]	T_L/T_S	301.15/300.15
Thermal diffusivity [m2/s]	α_L	$2.65\bullet10^{-5}$
Surface tension gradient [N/m.K]	σ_T	$8.4\bullet10^{-5}$
Latent heat [J/kg]	ΔH	243,500

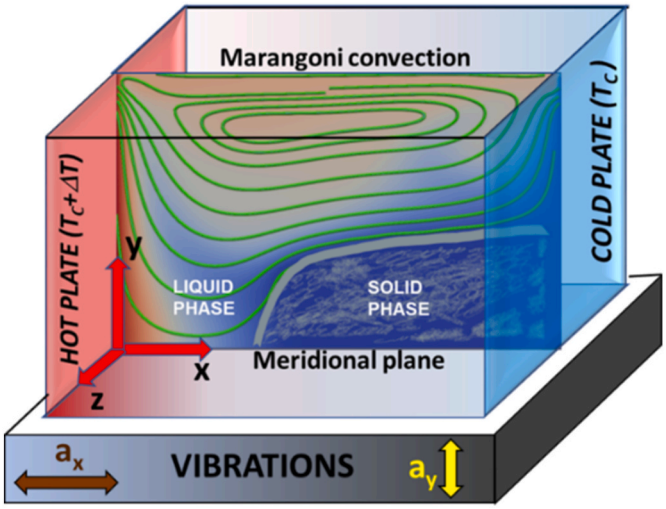

Fig. 1. Sketch of the parallelepipedic experimental cell and the meridional plane considered for the simulations.

study of the effectiveness of thermocapillary flows to increase the heat transfer rate in PCM systems [14,16]. Since the purpose of the MarPCM project is to perform the phase change (solid/liquid) experiment on the International Space Station (ISS), it is of the outmost importance to investigate how the vibratory environment affects/influences the experiment. Literature confirms that some fluid mechanics experiments conducted onboard ISS were affected by both residual and g-jitter accelerations, mainly the ones of low frequency [17–19]. Gaponenko et al. [20] studied the influence of harmonic external acceleration during the diffusion process of a binary mixture (water-isopranol) showing the strong interplay between gravity and vibrational impact. Khoshnevis et al. [21] analyzed the influence of g-jitter and residual accelerations during thermodiffusion IVIDIL experiment, where they used quasi-steady acceleration data from MAMs sensor (as residual accelerations) and SAMS data as g-jitter perturbation. Point out that, these signals correspond to a quiescent period of the ISS, without enhanced acceleration episodes. They detected that the thermodiffusion process was not influenced by residual accelerations but could be influenced by the low-frequency component of g-jitter. More recent studies introduced a real ISS acceleration signal containing a reboosting period during the thermodifussion experiment, DCMIX campaign. The authors concluded that during the diffusive phase there were errors in the determination of coefficients of diffusion in the ternary systems depending on the direction of the reboosting. These errors arose when the reboosting maneuver was acting perpendicular to the concentration gradient [22].

The objective of this paper is, thus, to analyze how the potential disturbances, g-jitters, can affect the thermocapillary flux as well as the solid/liquid interface evolution during the melting process of the *n*-octadecane, as PCM material. 2D simulations by using the parallelepipedic geometry and introducing a real acceleration signal coming from an ISS reboosting maneuver have been proposed by the authors. To predict the safety margins of the ISS experiment, different g-level scenarios have been considered by increasing the intensity of the reboosting up to 1000 times the real one. In addition, the influence of the direction of the reboosting, parallel (x direction) and perpendicular (y direction) to the thermal gradients, on the melting process has been as well evaluated in order to optimize the cell orientation onboard ISS.

2. Methodology and simulation details

The PCM material selected for this study was the *n*-octadecane (Prandtl number equal to 52.53) as it has the optimal properties for the melting process under microgravity conditions and successfully accomplish the ISS safety requirements. Its thermophysical properties are compiled in Table 1 [23,24].

The experimental cell proposed to be used onboard ISS has a parallelepipedic geometry with the following dimensions 22.5 × 15 × 25 mm. Thus, for the 2D simulations, the meridional plane with 22.5 × 15 mm (see Fig. 1) has been proposed. Initially, the *n*-octadecane was in the solid phase, with its temperature under the melting one ($T_{initial} = 298.15$ K). Once applied a ΔT ($T_{hot\ plate} - T_{cold\ plate}$) over the lateral walls a controlled solid-liquid phase change began.

2.1. Governing equations

To describe the melting process, the enthalpy-porosity method was employed [25–29]. Assuming the same density for both solid and liquid phases, the essence of this methodology is based on the definition of a scalar field, temperature depending, called the local liquid fraction *lf*. This scalar bounds between 0 – pure solid region – and 1 – pure liquid region –, coupling the momentum and energy balances (see eq. (1)).

$$l_f = 0 \ if \ T \le T_S$$

$$l_f = \frac{T - T_S}{T_L - T_S} \ if \ T_S < T < T_L \tag{1}$$

$$l_f = 1 \ if \ T \ge T_L$$

with T_S and T_L, the temperatures at which the system is in the solid and liquid state, respectively. The melting temperature is then defined as $T_m = (T_S + T_L)/2$ which means that the melting front is accordingly defined as $l_f = 0.5$.

Considering the liquid newtonian and incompressible, the momentum balance was described by following equations (see Refs. [25,26])

$$\nabla \boldsymbol{u} = 0 \tag{2}$$

$$\frac{\partial \boldsymbol{u}}{\partial t} + (\boldsymbol{u}\nabla)\boldsymbol{u} = -\frac{1}{\rho_0}\nabla p + \nu\nabla^2\boldsymbol{u} + \frac{1}{\rho_0}\frac{C(1-l_f)^2}{l_f^3 + b}\boldsymbol{u} + \boldsymbol{g} \tag{3}$$

$$\boldsymbol{u} = l_f \, \boldsymbol{u}_L \tag{4}$$

where $\boldsymbol{u}$ is the weighted velocity vector, $\boldsymbol{u}_L$ the liquid velocity vector, p the buoyant pressure (difference between total and hydrodynamic pressures), ν the kinematic viscosity of the liquid phase, ρ_0 the density at a reference temperature (T_L) and $\boldsymbol{g}$ represents the residual acceleration vector in the ISS including the reboosting period. The liquid fraction is included in the last term of equation (3), which models the solid-liquid interface as a partially melted region having its porosity given by this scalar field (l_f). The value of the permeability, or Darcy constant C, significantly influences the partially melted region characteristics. If the value of C is raised, the flow in that region lessens, leading to a reduction in the heat exchange and flattens the solidification front. Due to this, the value of C must be adjusted to match experiments and computational models (see Ref. [28]). In the present work the value of C has been fixed at 1.6×10^6 kg/m$^3\bullet$s, while the numeric constant b has been fixed at

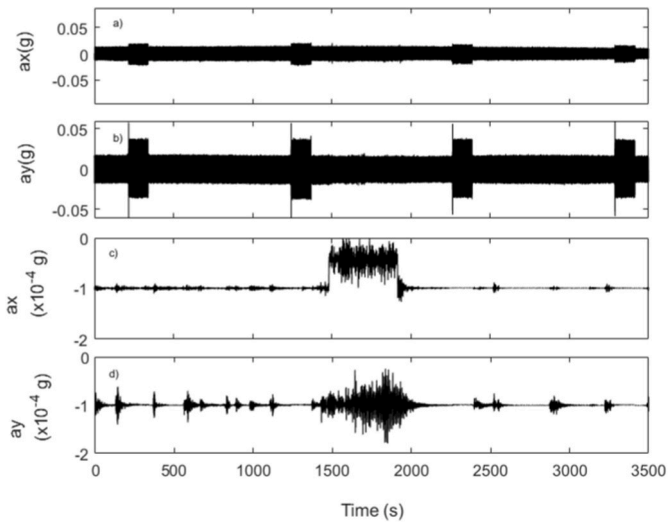

Fig. 2. Raw acceleration components in the x and y directions a) and b) and their corresponding denoised signals c) and d).

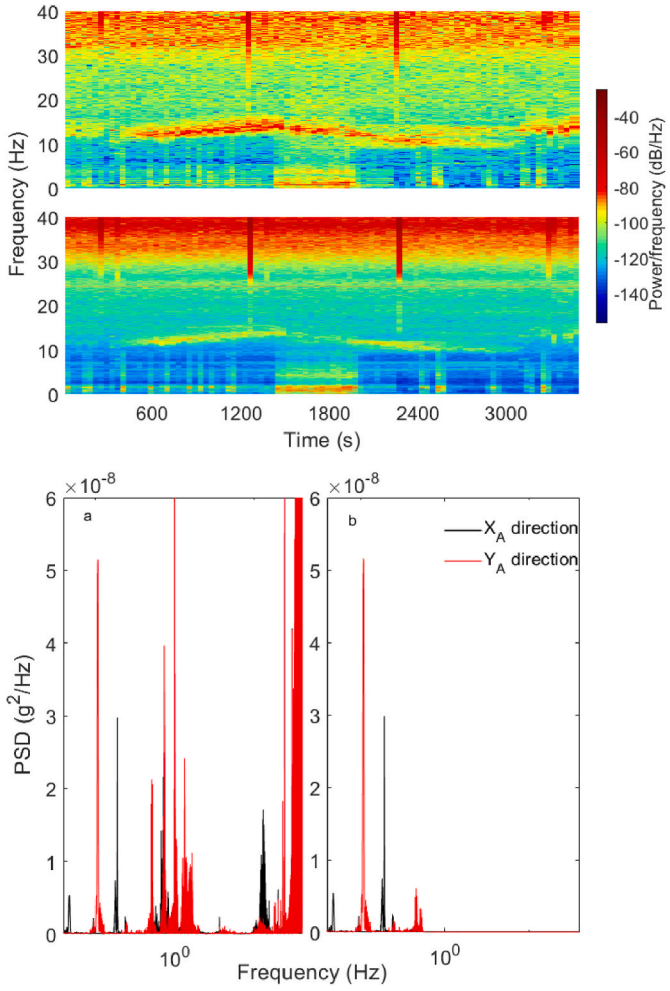

Fig. 3. a) The spectrograms and b) Power Spectral Density (PSD) of the x and y acceleration components. Left - original signal and right - denoised signal.

10^{-3} to avoid division by zero [27].

Concerning the energy equation, a new source term including both space and time derivatives of the liquid fraction is added,

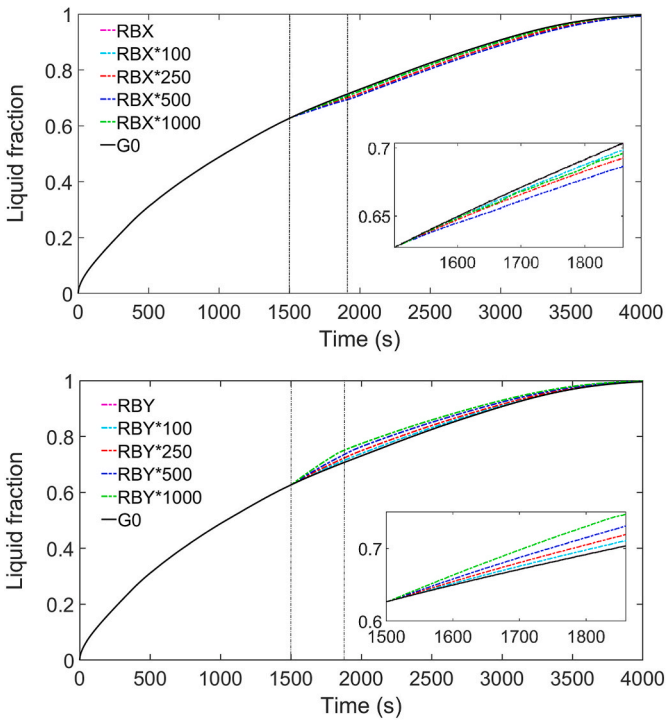

Fig. 4. The evolution of the liquid fraction of *n*-octadecane for all cases of real and increased g-dose a) in the x direction and b) in the y direction, compared to zero gravity case; the insets represent the magnification of the liquid fraction evolution including the reboosting period. The dashed vertical lines indicate the reboosting duration.

$$\frac{\partial c_p T}{\partial t} + (\boldsymbol{u}\nabla)c_p T = \frac{1}{\rho_0}\nabla(\lambda\nabla T) - \Delta H\frac{\partial l_f}{\partial t} \tag{5}$$

$$c_p = (1 - l_f)c_S + l_f c_L \tag{6}$$

$$\lambda = (1 - l_f)\lambda_S + l_f\lambda_L \tag{7}$$

where ΔH is the latent heat, c_p the weighted specific heat and λ is the weighted thermal conductivity. Subindexes S and L correspond to solid and liquid phase properties.

2.2. Numerical method

The temperature boundary conditions were set as T_L in the right side (cold wall) of the domain while in the left side (hot wall) the temperature was fixed at $T_L + \Delta T$. In the present simulation the temperature difference was considered 30 K in order to cover the worst-case scenario in terms of real experiment temperature requirements onboard ISS (maximum proposed $\Delta T = 25$ K – MarPCM project) [15,16]). The upper and lower sides of the domain were considered adiabatic. No-slip boundary conditions were systematically applied to all boundaries except in the upper one, the free surface, in which Marangoni convection was considered to drive the surface flow by thermocapillary forces (see equation (8)) due to the surface tension (σ) variation with temperature.

$$\mu\nabla_n \boldsymbol{u}_\tau = -\sigma_T\nabla_\tau T \tag{8}$$

$$\sigma_T = \frac{\partial\sigma}{\partial T} \tag{9}$$

where σ_T is the surface tension coefficient and μ the dynamic viscosity. n and τ denote the normal and tangential vector components to the free surface. Mention that the free surface has been considered perfectly flat.

The initial conditions were always kept the same, the whole domain

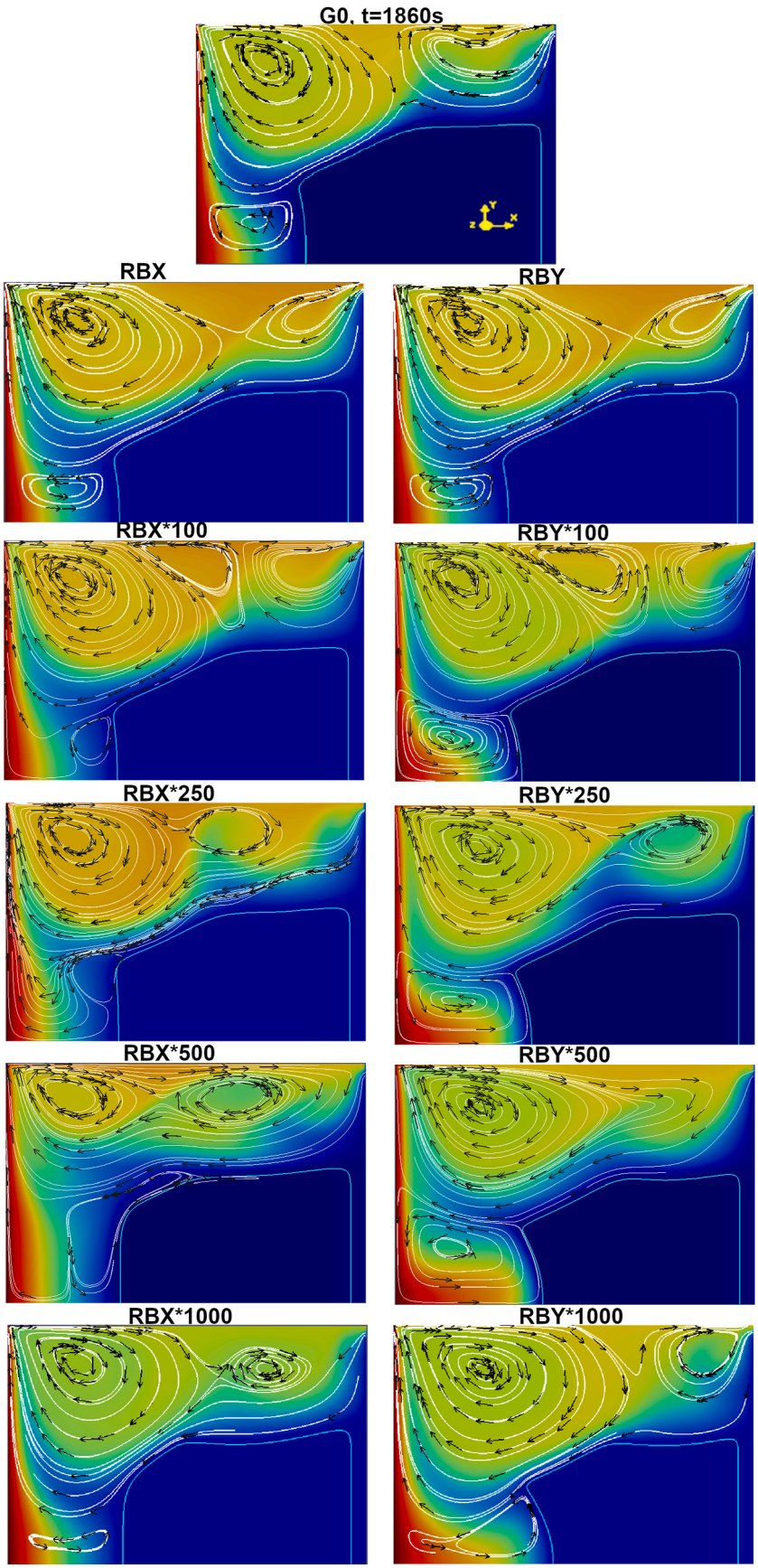

Fig. 5. Temperature and flow patterns of *n*-octadecane at t = 1860s (reboosting end time) along the meridional plain for all cases considered. Inset: the QR code for the full video of the flow.

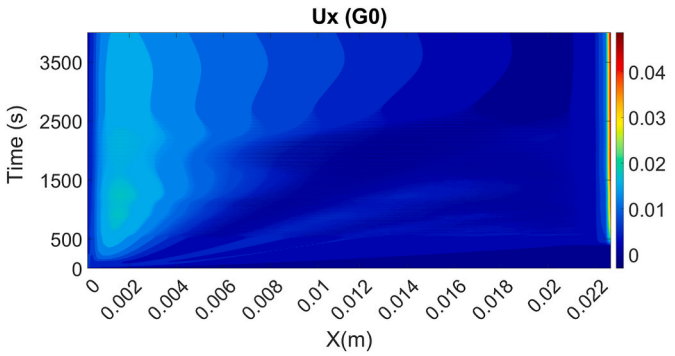

Fig. 6. Velocity (u_x) field along the free surface for quiescent period (G0).

was at rest and at the temperature $T_{initial}$.

The open access OpenFoam environment was selected to solve the above equations using second order schemes for both space and time discretization. The simulation time step was always fixed at 2 m s coinciding with the signal time steps. This adjustment was advantageous as implied no further signal manipulations to introduce the acceleration data in the calculations. The momentum and continuity equations were solved using the PIMPLE algorithm, a blended scheme between PISO and SIMPLE algorithms that ensures a correct coupling between the pressure and the velocity. The temperature was calculated in each PIMPLE iteration. The final system of linear equations was solved using the preconditioned bi-conjugate gradient, PBiCG, method with a common tolerance of 10^{-8} for pressure, velocity and temperature fields [25,26,29,30].

For testing numerical convergence three different rectangular meshes have initially been considered with elementary cell dimensions of 0.15 × 0.10 (coarse), 0.09 × 0.075 (intermediate) and 0.0625 × 0.05 (fine) mm^2, respectively. Considering as adjusting parameter the global liquid fraction evolution, the results obtained with the intermediate mesh offered an excellent compromise because the difference against the fine mesh was below 2.8 % on average. To lower even more this percentage, the intermediate mesh was further refined near the free surface and the lateral hot wall, where the gradients of the physical magnitudes are expected to intensify. More details about the applied method and convergence tests can be found in the literature [31].

2.3. Acceleration signal details

As the ISS MarPCM experiment is still pending to be scheduled, for the present work an older acceleration signal containing a typical ISS reboosting period has been considered in order to analyze the most unfavorable vibratory scenario. Remark that the maximum acceleration levels can be reached during this kind of maneuvers [32,33]. The signal associated to the reboosting maneuver performed on the June 24, 2021 was selected as representative for the simulations. The reboosting lasted a long period (445 s) by using the DC-177 P Mid-Ring thrusters and resulting in a g-dose of about $\Delta v = 0.5$ m/s (mean acceleration level of 122 μg). The selected signal was recorded by 121f03 SAMS sensor, located in the US laboratory module, Lab 101 in the ER2 lower Z panel [34], with the sampling rate of 500 data per second which equivalates to a time step of 0.002 s. Notice that, this time step coincides with the time step needed to complete the simulations. The duration of the raw signal was about 22 h.

As demonstrated before [22] the low frequency range showed to be the most harmful for the fluid mechanics experiments, therefore, the above signal was cleared of high frequency components by applying a denoise technique, in which was used a symlet 8 function as mother wavelet with a decomposition level of 9. This procedure filtered the signal for frequencies under 1 Hz (more details in Ref. [35]. Since the *n*-octadecane melting process lasted around 4000 s, the denoised signal was cut accordingly, matching the onset of the reboosting to coincide the 1500 s after the melting process began. Fig. 2 plots the raw (a, b) and denoised (c, d) acceleration components in the x and y directions (ISS x_A and y_A absolute coordinates), clearly showing the reboosting period location and its intensity. To assure that the denoise process has been done correctly, the spectrograms of the original and denoised signals of both x and y acceleration components together with their Power Spectral Density (PSD) were plotted in Fig. 3. Remark that, hereinafter, the x acceleration component will be called the active component of the reboosting. The PSD was based on the Welch method which splits the signal into overlapping time windows and averages the results to give the final power spectral density representation. The spectrogram was represented minute by minute so that the reboosting period can be clearly detected. More details about the method can be found in the literature [36–38]. Certainly, after applying the denoise algorithm, the remaining spectral content of the reduced signal was under 1 Hz.

3. Results and discussion

The influence of the reboosting maneuver on the melting process is analyzed by using three complementary variables: the evolution of the solid/liquid fraction, the dynamics of the flow and its oscillatory regime.

To do so, two reboostings scenarios have been proposed: the first one, the reboosting signal was introduced with the active acceleration component (a_X, see Fig. 2c) parallel to the thermal gradient direction (x direction) denoted as RBX. In the second scenario, the acceleration vector was introduced with the reboosting active component perpendicular to the thermal gradient direction (y direction) and was labelled RBY. Moreover, to study the influence of the g-dose on the melting process the authors proposed five levels of reboosting intensity, ranging from the real data (RBX and RBY) up to 1000 times the real values (0.2 g or 2 m/s^2), multiplying only the real reboosting period by 100 (RBX/RBY*100), 250 (RBX/RBY*250), 500 (RBX/RBY*500) and 1000 (RBX/RBY*1000), respectively.

Fig. 4 plots the temporal evolution of the liquid fraction during the melting process of *n*-octadecane for the five different g-level conditions specified earlier (dashed lines) and considering the two reboosting scenarios introduced earlier. For comparison, the zero gravity environment was as well presented as a solid line (case G0). Fig. 4a and b correspond to RBX and RBY cases, respectively. The reboosting period takes place between 1500 s and 1860 s and is indicated by the two dashed vertical lines. The insets crop the liquid fraction evolution from the onset of the reboosting period until the end in order to give a magnified view of how each of the g-doses selected affect the melting process. As can been seen the dynamics of the melting remained unaffected for real reboosting cases (RBX and RBY) though by increasing significantly the g-dose an appreciable change in the melting process has been detected. With regard to RBY*1000 case the deviation of the liquid fraction evolution respect to the G0 one, reached 6 % (see Fig. 4 b, inset), while for RBX*1000 this difference was lower.

The simulations point out that the phase change interface depended on the location of the vortex centers that appeared in each case study (see Fig. 5). It can be observed the presence of the vortical structures produced by the Marangoni convection which favored the temperature homogenization near the free surface compared to the lower part of the domain. The latter results were in agreement with those published in the literature for low aspect ratios [39].

The temperature distribution presented different patterns depending on the direction of the active reboosting component. On the one hand, analyzing the RBY simulations, if the g-doses was increased from 250 up to 1000 times the real g-dose, appreciable changes in the flow patterns have been detected due to the fact that the hot material concentrated in the left lower corner. This could be explained by the existence of the upward acceleration during the reboosting that moves the hot material downward. This movement produced by the buoyancy, favored the melting in this area, changing the shape of the interface (see Fig. 5). On

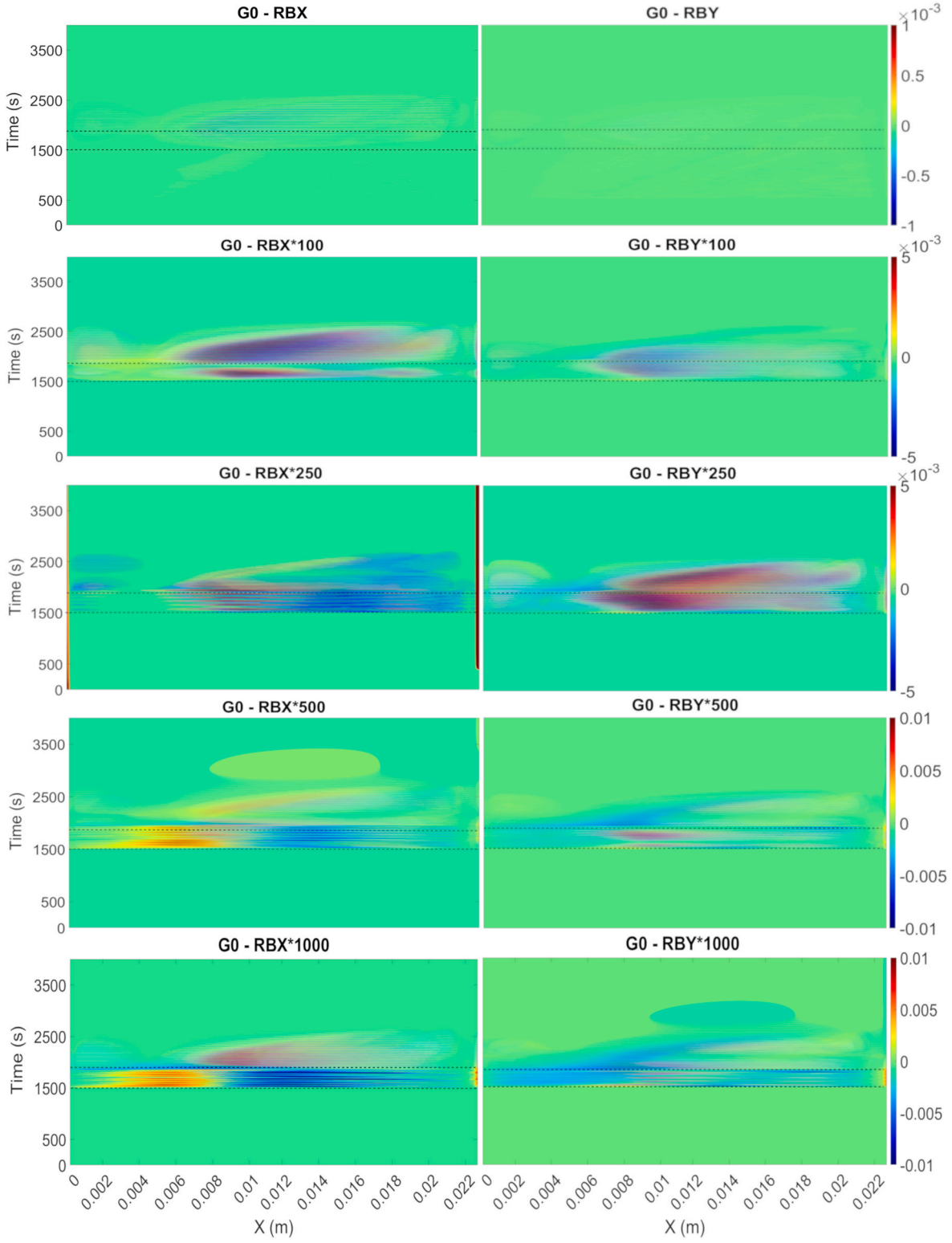

Fig. 7. Velocity field differences along x direction (u_x) for all cases of reboosting intensity with respect to the zero gravity cases. The parallel dashed lines point out the reboosting period.

the other hand, the reboosting on x direction had less effect on the melting inducing minor interface alterations in its upper-left part. This could be explained by the weak interaction between the dominant vortex and solid phase. A full visualization of the thermal and dynamic fields is available scanning the QR codes included in Fig. 5.

To complement the above results the time evolution of the x component of the velocity, along the x direction, at the free surface (u_x) in all reboosting cases were analyzed. As an example, Fig. 6 plots the u_x for the G0 case. Note that, the velocity was generated by Marangoni effect as a consequence of the gradual increase of the liquid fraction at the surface. Its maximum magnitude was reached when the free surface was entirely liquid (approximately 400 s) and this value was maintained

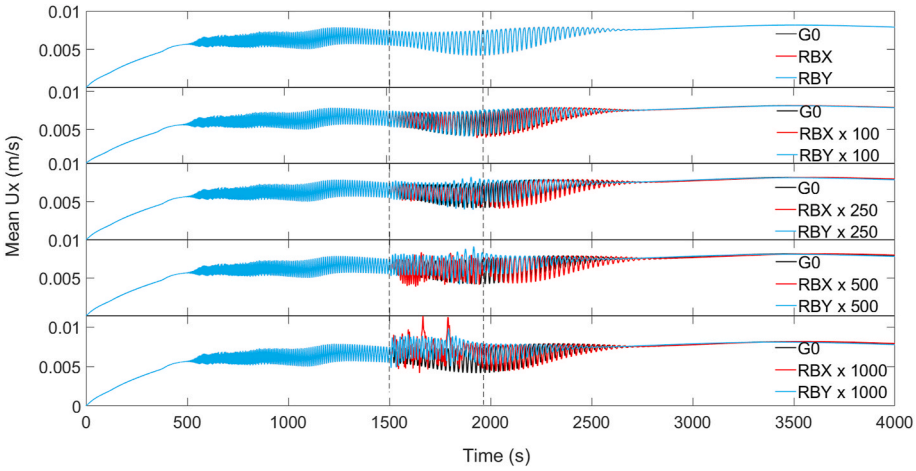

Fig. 8. Time evolution of the mean velocity in the x direction at the free surface for all cases studied.

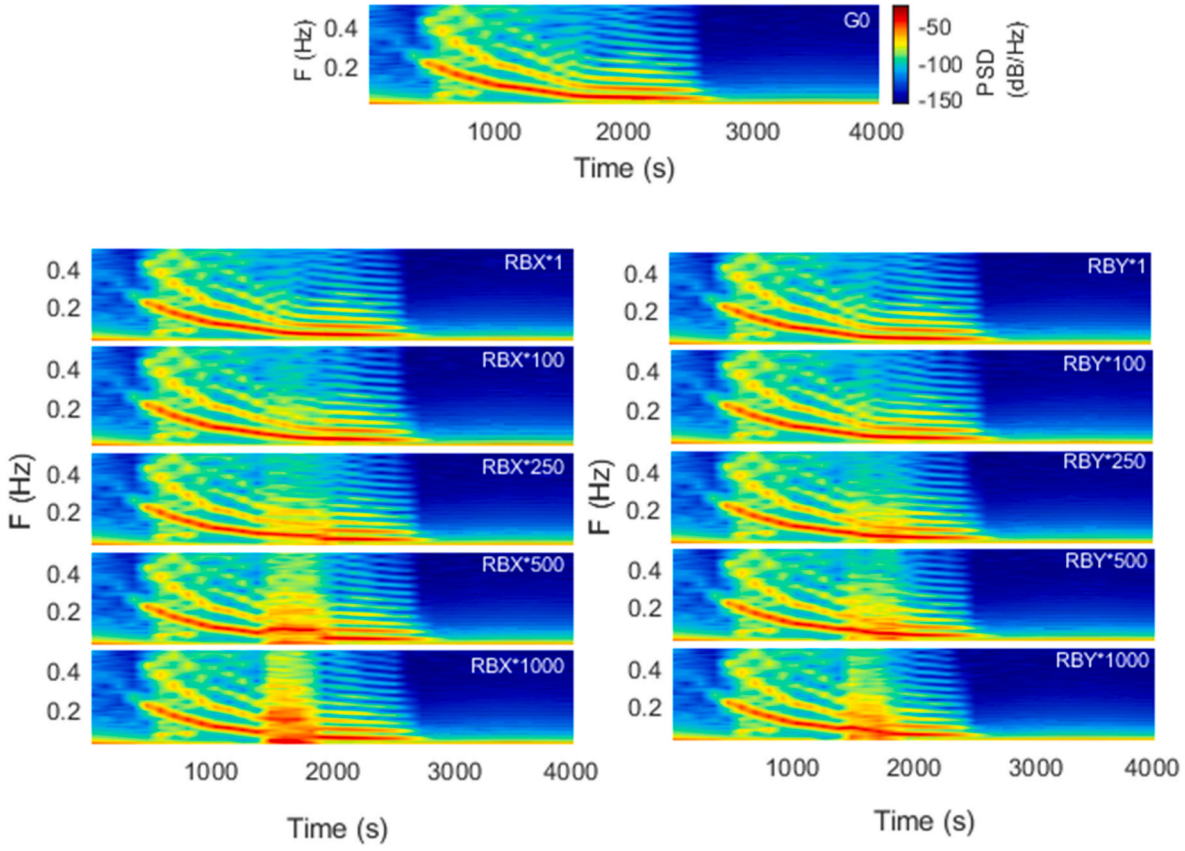

Fig. 9. Spectrograms of the mean u_x values for all cases studied.

during the melting process. The highest values of the u_x were detected close to the hot wall which were implicitly related to the development of the main vortex.

To analyze the influence of the g-jitter on the latter velocities at free surface, a quantitative analysis based on the u_x differences between G0 levels and all the reboosting cases has been considered (see Fig. 7). No significant differences were obtained for RBX and RBY cases, although, by increasing the g-levels changes in the u_x during the reboosting period and beyond it have been observed. In other words, by applying a higher reboosting intensity, specially acting parallel to the thermal gradient, the Marangoni effect was altered. Considering the real acceleration level though, no effect on the thermocapillary convection has been detected.

The characterization of the oscillatory regime of each of the cases studied above has been thought to complement the dynamics of the melting process and give a deeper understanding of how the reboosting maneuver could affect the melting. Fig. 8 compares the time evolution of the mean value of the velocity component in the x direction, at the free surface, under microgravity conditions to different g-dose levels. It can be noticed an increase in the mean u_x values fluctuations at the onset of the reboosting and during the whole maneuver if the acceleration is equal or larger than 500 times than the real one. Hence, the oscillatory regime was more sensitive to the perturbations induced by the maneuvers in the x direction. This is in concordance with the results presented in Fig. 7. Moreover, the perturbations in the oscillatory regime found

earlier, continued approximately 1000 s post reboosting process until they disappeared.

The above stated, was corroborated by analyzing the spectrograms of the mean u_x values, represented in Fig. 9. It can be spotted, sudden changes in the mean u_x main frequency during the reboosting maneuver, mainly if the high g-levels of acceleration were considered (>250 times real g-level). This fact has been observed in both x and y direction reboosting scenarios and can be explained by the increasing complexity of the flow patterns at high g-levels (see Fig. 6 inset).

4. Conclusions

A parametric analysis of the dynamic of the melting process and the oscillatory regime of the velocity field under different g-dose of the reboosting induced in both x and y directions has been studied.

The melting process showed to be unaltered if a real reboosting perturbation is to be applied (order of 10^{-4} g) independently of the cell orientation respect to the reboosting maneuver. However, increasing the reboosting intensity (up to 1000 times higher), it might disturb the experiment. For RBX simulations, the results showed that the dynamic of the melting was maintained even if the acceleration levels have been increased by a factor of 1000. Nevertheless, if the active acceleration component was applied in y direction, the melting process was more affected and the shape of the solid-liquid interface more altered, if high g-doses were applied. In contrast, the time evolution of the mean u_x at the free surface showed that the alterations during its oscillatory regime were more relevant if the active reboosting component was introduced in the x direction and higher g-levels were considered. In addition, these perturbations affect the period post reboosting and smoothly returns to the zero gravity pattern.

To wrap up, the melting process may be affected if considerable high g levels are to be induced. The real reboosting g-levels that are applied to correct the ISS orbit will not affect the experiment and the orientation of the experimental cell inside the ISS is not a critical factor to be taken into account.

Declaration of competing interest

The authors declare that they have no known competing financial interests or personal relationships that could have appeared to influence the work reported in this paper.

Acknowledgements

This work was supported by the Ministerio de Ciencia e Innovación (MICIU/Feder) under the Project PID2020-115086 GB-C32 and Rovira I Virgili University grant (2023PFR-URV-00148).

Appendix A. Supplementary data

Supplementary data to this article can be found online at https://doi.org/10.1016/j.actaastro.2023.12.020.

References

[1] M. M Farid, A. Auckaili, S.A.K. Razack, S. Al-Hallaj, A review on phase change energy storage: materials and applications, Energy Convers. Manag. 45 (2004) 1597–1615.
[2] K. Pielichowska, K. Pielichowski, Phase change materials for thermal energy storage, Prog. Mater. Sci. 65 (2014) 67–123.
[3] S. Nagar, P.K. Singh, A short review on the industrial applications of phase change materials, IOP Conf. Ser. Mater. Sci. Eng. 1116 (2021), 012006.
[4] M.I. Lone, R. Jilte, A review of phase change materials for different applications, Mater. Today: Proccedings 46 (2021) 10980–10986.
[5] M. Tawalbeh, H. Khan, A. Al Othman, F. Almomani, A comprehensive review on the recent advances in materials for thermal energy storage applications, Int. J. Thermofluids 18 (2023), 100326.
[6] J.P. Collette, P. Rochus, R. Peyrou-Lauga, O. Pin, N. Nutal, M. Larnicol, J. Crahay, Phase Change Material Device for Spacecraft Thermal Control, IAC Congress, 2011. IAC-11.C2.8.1.
[7] A. Kumar, A. Sekar, D.N. Siddhartha Jain, K.V. Govinda, Phase change materials (PCM) for thermal control during spacecraft transportation, Int. J. Mech. Ind. Eng. 3 (2014) 235–239.
[8] S.F. Morea, The lunar roving Vehicle: historical perspective, Second Conf. Lunar Bases and Space Activities of the 21st Century 2 (1992) 619–632.
[9] R. Barzin, J.J.J. Chen, B.R. Young, M.M. Farid, Application of PCM energy storage in combination with night ventilation for space cooling, Appl. Energy 158 (2015) 412–421.
[10] M. Izenson, D. Knaus, F. Valentin, J. Sanders, Lightweight, durable PCM heat exchanger for spacecraft thermal control, in: 47th International Conference on Environmental Systems, ICES-2017-055, July 2017, pp. 16–20.
[11] I. Garmendia, H. Vallejo, M. Seco, E. Anglada, Design and fabrication of a phase change material heat storage device for the thermal control of electronics components of space applications, Aerospace 9 (2022) 126.
[12] J.M. Ezquerro, A. Bello, P. Salgado Sanchez, A. Laverón-Simavilla, V. Lapuerta, The thermocapillary effects in phase change materials in microgravity (TEPim) experiment: design, preparation and execution of a parabolic flight experiment, Acta Astronaut. 162 (2019) 185–196.
[13] J.M. Ezquerro, P. Salgado Sanchez, A. Bello, J. Rodríguez, V. Lapuerta, A. Laverón-Simavilla, Experimental evidence of thermocapillarity in phase change materials in microgravity: measuring the effect of Marangoni convection in solid/liquid phase transitions, Int. Commun. Heat Mass Tran. 113 (2020), 104529.
[14] P. Salgado Sanchez, J.M. Ezquerro, J. Porter, J. Fernandez, I. Tinao, Effect of thermocapillary convection on the melting of phase change materials in microgravity: experiments and simulations, Int. J. Heat Mass Tran. 154 (2020), 119717.
[15] J. Porter, A. Laverón-Simavilla, M.M. Bou-Ali, X. Ruiz, Jna Gavaldá, D. Dubert, J. M. Ezquerro, J. Fernández, L. García-Fernández, D. Gligor, J. Gomez, V. Lapuerta, U. Martinez, J. Massons, J. Rodriguez, P. Salgado Sánchez, A. Sanjuan, B. Seta, V. Shevtsova, I. Tinao, The effect of Marangoni convection on heat transfer in phase change materials experiment. 27th ELGRA biennial symposium and general assembly, Book of Abstracts 77–78 (2022).
[16] J. Porter, A. Laveron-Simavilla, M. Mounir Bou-Ali, X. Ruiz, Jna Gavalda, J. M. Ezquerro, P. Salgado Sanchez, U. Martinez, D. Gligor, I. Tinao, J. Gomez, J. Fernandez, J. Rodriguez, A. Borshchak-Kachalov, V. Lapuerta, B. Seta, J. Massons, D. Dubert, A. Sanjuan, V. Shevtsova, L. García-Fernández, The "effect of Marangoni convection on heat transfer in phase change materials" experiment, Acta Astronaut, Volume 210, pages: 212-223, (2023).
[17] X. Ruiz, P. Bitlloch, L. Ramírez-Piscina, J. Casademunt, Impact of stochastic accelerations on dopant segregation in microgravity semiconductor crystal growth, J. Cryst. Growth 355 (2012) 88–100.
[18] O. Sánchez, X. Ruiz, M. Pujalte, I. Mercader, O. Batiste, Jna Gavaldà, On the determination of interdiffusion coefficients in liquid binary alloys and doped semiconductors. Several implications concerning the International Space Station, Int. J. Heat Mass Tran. 86 (2015) 508–518.
[19] N. Sáez, X. Ruiz, J. Pallarés, V. Shevtsova, On the accuracy of the interdiffusion coefficient measurements of high temperature binary mixtures under real ISS conditions, Compt. Rendus Mec. 341 (2013) 405–416.
[20] Y. Japonenko, V. Shevtsova, Effects of vibrations on dynamics of miscible liquids, Acta Astronaut. 66 (1–2) (2010) 174–182.
[21] A. Khoshnevis, A. Ahadi, M.Z. Saghir, On the influence of g-jitter and prevailing residual accelerations onboard International Space Station on a thermodiffusion experiment, Appl. Therm. Eng. 68 (2014) 36–44.
[22] R. Jurado, J. Pallarés, Jna Gavaldà, X. Ruiz, Effect of reboosting maneuvers on the determination of Soret coefficients of DCMIX ternary systems, Int. J. Therm. Sci. 142 (2018) 205–219.
[23] N. García-Acosta, P. Salgado Sanchez, J. Jimenez, U. Martínez, J.M. Ezquerro, Thermocapillary-enhanced melting of different phase-change materials in microgravity, Microgravity Sci. Technol. 34 (2022) 92.
[24] R. Varas, P. Salgado Sánchez, J. Porter, J.M. Ezquerro, V. Lapuerta, Thermocapillary effects during the melting in microgravity of phase change materials with a liquid bridge geometry, Int. J. Heat Mass Tran. 178 (2021), 121586, https://doi.org/10.1016/j.ijheatmasstransfer.2021.121586. ISSN:0017-9310.
[25] B. Šeta, D. Dubert, M. Prats, Jna Gavaldà, J. Massons, M.M. Bou-Ali, X. Ruiz, V. Shevtsova, Transition between nonlinear regimes in melting and liquid bridges in microgravity, Int. J. Heat Mass Tran. 193 (2022), 122984.
[26] B. Šeta, D. Dubert, J. Massons, Jna Gavaldà, M.M. Bou-Ali, X. Ruiz, Effect of Marangoni induced instabilities on a melting bridge under microgravity conditions, Int. J. Heat Mass Tran. 179 (2022), 121665.
[27] S. Madruga, N. Haruki, A. Horibe, Experimental and numerical study of melting of the phase change material tetracosane, Int. Commun. Heat Mass Tran. 98 (2018) 163–170.
[28] S. Madruga, C. Mendoza, Enhancement of heat transfer rate on phase change materials with thermocapillary flows, Eur. Phys. J. Spec. Top. 226 (2017) 1169–1176.
[29] S. Madruga, G.S. Mischlich, Melting dynamics of a phase change material (PCM) with dispersed metallic nanoparticles using transport coefficients from empirical and mean field models, Appl. Therm. Eng. 124 (2017) 1123–1133.
[30] S. Madruga, C. Mendoza, Heat transfer performance and melting dynamic of a phase change material subjected to thermocapillary effects, Int. J. Heat Mass Tran. 109 (2017) 501–510.

[31] B. Seta, P. Salgado Sanchez, J. Massons, Jna Gavalda, M.M. Bou-Ali, Jeff Porter, X. Ruiz, V. Shevtsova, Three-dimensional effects during the melting of phase-change materials with thermocapillary flow in microgravity, in: Proceedings of the 27th European Low Gravity Research Association Biennial Symposium and General Assembly, 2022, pp. 52–53. Lisbon.
[32] M. Marín, D. Dubert, M.J. Simon, J. Ollé, Jna Gavalda, X. Ruiz, ISS quasi-steady accelerometric data as a tool for the detection of external disturbances during the period 2009-2016, Microgravity Sci. Technol. 30 (2018) 611–624.
[33] P.I.M.S. Nasa. https://gipoc.grc.nasa.gov/wp/pims/handbook/. https://gipoc.grc.nasa.gov/pims/pimsdocs/public/ISS%20Handbook/hb_vib_vehicle_Progress_77P_Reboost_2021-06-24.pdf. Last acces 3rd of October 2023.
[34] P.I.M.S. Nasa. https://gipoc.grc.nasa.gov/pims/pub/pad/year2021/month06/day24/. Last acces 3rd of October 2023.
[35] R. Jurado, Jna Gavaldà, M.J. Simón, J. Pallarés, A. Laverón-Simavilla, X. Ruiz, V. Shevtsova, Some considerations on the vibrational environments of the DSC-DCMIX1 experiment onboard ISS, Acta Astronaut. 129 (2016) 345–356.
[36] J. Ollé, D. Dubert, Jna Gavaldà, A. Laverón-Simavilla, X. Ruiz, V. Shevtsova, Onsite vibrational characterization of DCMIX2/3 experiments, Acta Astronaut. 140 (2017) 409–419.
[37] J. Ollé, R. Jurado, D. Dubert, Jna Gavaldà, A. Laverón-Simavilla, X. Ruiz, V. Shevtsova, Characterization of the accelerometric environment of DCMIX2/3 experiments, Microgravity Sci. Technol. 30 (2018) 683–697.
[38] D. Dubert, M. Marin-Genescà, M.J. Simón, J.M. Ezquerro, J. Massons, Jna Gavaldà, X. Ruiz, V. Shevtsova, On the monitoring of the vibratory environment of DCMIX4 campaign. Preliminary results, Microgravity Sci. Technol. 32 (2020) 615–628.
[39] P. Salgado Sánchez, J.M. Ezquerro, J. Fernández, J. Rodríguez, Thermocapillary effects during the melting of phase-change materials in microgravity: steady and oscillatory regimes, J. Fluid Mech. (2021) 908.